

# Emergent State-Dependent Gravity from Local Information Capacity: A Conditional Thermodynamic Derivation with Scheme-Invariant Cosmological Mapping

[clg]<sup>1</sup>

<sup>1</sup>[TBD Institution(s)]  
(Dated: August 28, 2025)

**Core hypothesis.** Each proper frame carries a finite quantum information capacity. Approaching this bound triggers a *state-dependent response* that preserves causal stitching with neighboring frames. *Kinematics remain GR-like:* we do not alter null geometry used by EM/GW luminosity distances. The response is *dynamical* (weak-field coupling), not kinematical (no extra time dilation beyond GR).

**Scope and conditionality.** All quantitative claims are conditional on a single working assumption: (A2) the Clausius relation  $\delta Q = T \delta S$  with Unruh normalization holds for small, near-vacuum local Rindler wedges (the *safe window*). We prove this relation holds to working order  $\mathcal{O}(\ell^4)$  with  $\mathcal{O}(\ell^6)$  corrections (Theorem 1). Within this regime we establish an *equivalence principle for modular response* (EPMR): after mutual-information subtraction with *moment-kill*, the  $\ell^4$  modular coefficient equals the flat-space value at working order, while curvature dressings enter at  $\mathcal{O}(\ell^6)$ . See Theorem 1 for the working-order statement and error control.

**Main outcomes.** (i) A microscopic sensitivity  $\beta$  from MI-subtracted modular Hamiltonians in flat-space QFT (Casini–Huerta–Myers balls, Osborn–Petkou normalization); (ii) a once-and-for-all geometric normalization with *continuous-angle invariance* showing only the *product*  $\beta f c_{\text{geo}}$  is physical; (iii) a *conditional, scheme-invariant mapping*  $\Omega_\Lambda = \beta f c_{\text{geo}}$  for the FRW zero mode; and (iv) a weak-field flux law with a universal geometric prefactor  $5/12$ , implying  $a_0 = (5/12) \Omega_\Lambda^2 c H_0$ . We keep the distance sector GR-like ( $\alpha_M = 0$  there), and we *enforce*  $|d_L^{\text{GW}}/d_L^{\text{EM}} - 1| \leq 5 \times 10^{-3}$ .

**Consequences.** With no cosmological inputs,  $\Omega_\Lambda = \beta f c_{\text{geo}} \approx 0.685$  and  $a_0 = (5/12) \Omega_\Lambda^2 c H_0$ . An *entropic state-action* law ( $\Delta S \geq 0$ ) determines a monotone  $\varepsilon(a)$  that modulates the weak-field response  $\mu(\varepsilon) = 1/(1 + \eta \varepsilon)$  with  $\eta = 5/12$ , suppressing growth and yielding  $S_8 \simeq 0.788$  ( $-7.4\%$  vs.  $\Lambda$ CDM), while EM/GW distances remain GR-like. An *illustrative, capped* environment-gated application to a SH0ES-like catalog nudges  $H_0 : 73.0 \rightarrow 71.32$  (SN cap only) and to 70.89 (SN+small Cepheid term), trending toward TRGB/Planck without altering null geometry. Explicit falsifiers and hygiene checks are stated.

## I. INTRODUCTION: CORE INSIGHT AND CONDITIONAL SCOPE

*a. High level summary.* We hypothesize that the geometric side of Einstein’s equations exhibits a *local, state-dependent response* because each small spacetime wedge has finite information capacity. As capacity is approached, the Clausius relation enforces a compensating response so adjacent wedges remain causally stitched. *Kinematics (null cones, EM/GW distances) stay GR-like;* all changes are *dynamical* (response strength in weak fields). Jacobson’s horizon thermodynamics is recovered as the stationary-horizon special case. All claims here are conditional on (A2); if (A2) fails, the construction must be revised. Our working-order result is stated as Theorem 1 (App. K).

*b. GR limit (distance sector).* In the limit of constant information capacity  $\nabla_a M^2 = 0$  (equivalently  $\alpha_M \rightarrow 0$ ), the construction collapses to standard GR — recovering Einstein’s equations with  $c_T = 1$  and GR light-cone geometry. Throughout we *keep*  $\alpha_M = 0$  *in the distance sector* and confine any late-time variation to the growth/response sector (Sec. X).

*c. State variable and coupling.* We define a dimensionless state variable  $\varepsilon(x)$  encoding fractional deviations of local capacity from its vacuum reference and parameterize

$$\frac{\delta G}{G} = -\beta \delta \varepsilon(x), \quad (1)$$

with  $\beta$  calculable from flat-space QFT (Sec. IV). The weak-field response is encoded by

$$\mu(\varepsilon) \equiv \frac{G_{\text{eff}}}{G_N} = \frac{1}{1 + \eta \varepsilon}, \quad \eta = \frac{5}{12}, \quad (2)$$

so  $\mu \rightarrow 1$  in strong fields (GR recovery) and  $\mu < 1$  in weak fields (gentle dynamical slowdown).

*d. Why  $\eta = \frac{5}{12}$ .* The coefficient follows from the same unit–solid–angle Noether normalization used in the FRW zero mode. Coarse-graining the  $\nabla \nabla M^2$  terms over the CHM wedge family yields a quasilinear flux law with a universal boundary–segment ratio; the isotropic null contraction contributes  $(4/3)$  and the segment geometry contributes  $(5/16)$ , giving  $(4/3) \times (5/16) = 5/12$ . Appendix L shows the identical factor fixing the static acceleration scale  $a_0 = (5/12) \Omega_\Lambda^2 c H_0$ ; using the same bookkeeping in the weak-field  $\mu(\varepsilon)$  guarantees scheme/angle invariance.

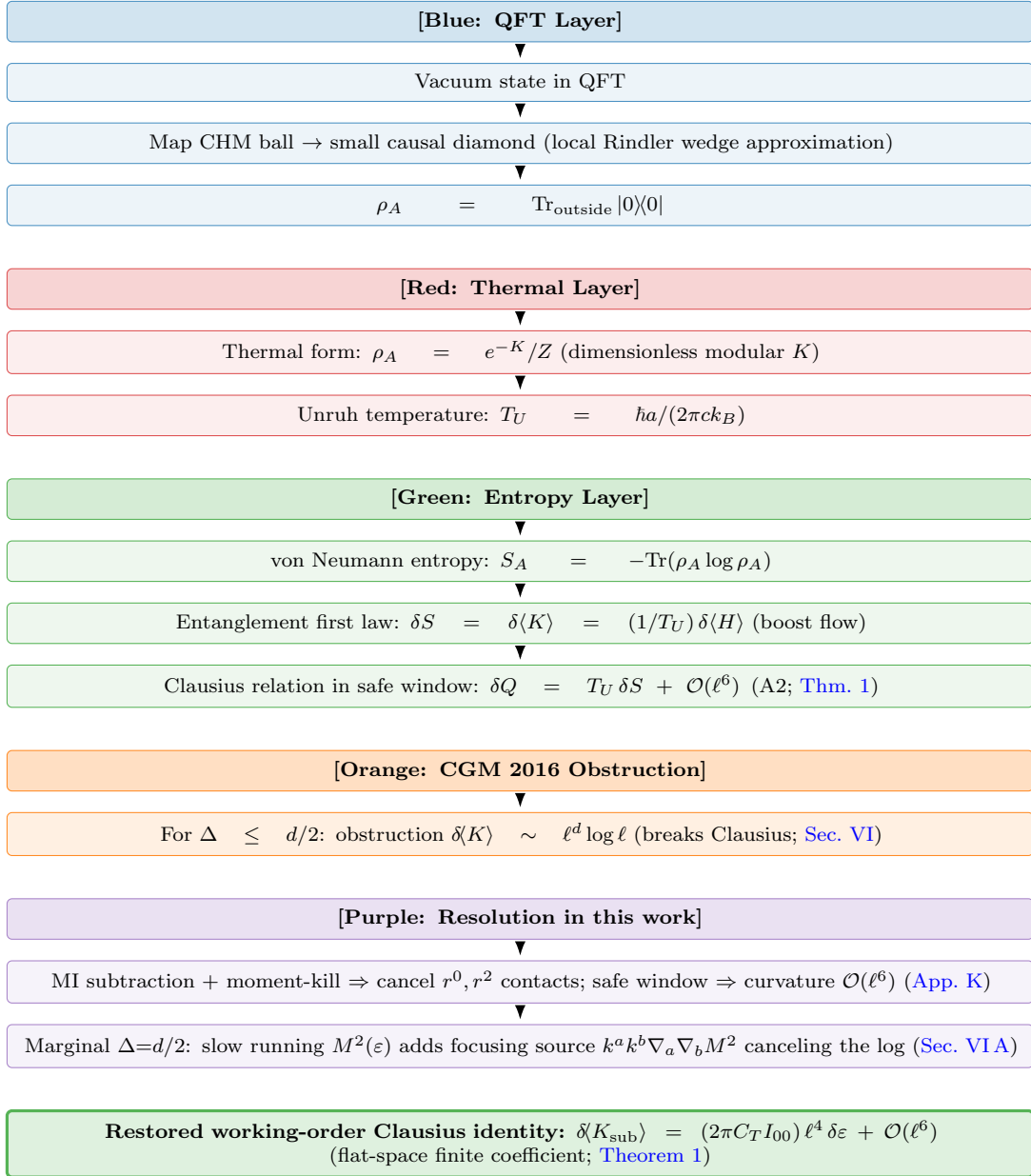


FIG. 1. Conceptual flow from QFT vacuum reduction to the working-order Clausius identity, highlighting the CGM (2016) obstruction and the resolution used here. Colors match later sections; placed early to orient readers.

*e. What is fixed vs. what is assumed. Fixed once:* wedge family (ball→diamond), generator density, Unruh normalization, unit–solid–angle boundary factor. *Assumed:* (A2) Clausius with Unruh in the *safe window* (Def. 1); Hadamard state; small perturbations. *Consequence:* the geometric mapping is *angle-invariant* (Sec. VII A); only  $\beta f c_{\text{geo}}$  is physical.

*f. Clean mapping statement.* Within the safe window and EPMPR working order, the FRW zero mode satisfies the *conditional, scheme-invariant* relation

$$\Omega_\Lambda = \beta f c_{\text{geo}}. \quad (3)$$

## II. ASSUMPTIONS AND DOMAIN OF VALIDITY

**Definition 1** (Safe window). Choose  $\ell$  obeying  $\epsilon_{UV} \ll \ell \ll \min\{L_{\text{curv}}, \lambda_{\text{mfp}}, m_i^{-1}\}$  for fields treated as massless; work with Hadamard states and small perturbations (relative entropy  $\mathcal{O}(\epsilon^2)$ ). Within this window the MI-subtracted, moment-killed modular response is dominated by  $\ell^4$  and admits a Clausius balance with Unruh normalization.

**Hypothesis 1** ((A2) Clausius with Unruh in the safe window). In the safe window,  $\delta Q = T \delta S$  with Unruh temperature holds for Casini–Huerta–Myers (CHM) diamonds mapped from balls, with flux built from  $T_{kk}$  along approximate generators.

*a. Working-order theorem.* Assuming Lemmas H.1–H.2 and Proposition H.1 (App. K), the small-diamond Clausius identity holds to  $\mathcal{O}(\ell^4)$  with  $\mathcal{O}(\ell^6)$  corrections; cf. Theorem 1. The marginal  $\Delta = d/2$  compensator is summarized in Lemma 1.

*b. First-law domain.* We use  $\delta S = \delta \langle K \rangle$  only for CHM balls/diamonds and small perturbations of a Hadamard state; no general wedge theorem is claimed.

### A. Failure modes of (A2) and explicit falsifiers

(A2) could fail if: (i) MI-subtracted flat-space modular data do not transfer to null diamonds; (ii) Unruh normalization fails in small, non-stationary wedges; or (iii) nonlocal state dependence spoils the local Clausius balance. Falsifiers (Sec. XII): (a) GW/EM luminosity distance ratios inconsistent with bounded  $\alpha_M$ ; (b) laboratory/solar-system bounds revealing  $|\dot{G}/G| \gtrsim 10^{-12} \text{ yr}^{-1}$ ; (c) precision cosmology favoring  $\Omega_\Lambda$  inconsistent with the invariant  $\beta f c_{\text{geo}}$ .

### B. Pre-commitment and scheme invariance (convention hygiene)

We *pre-commit* to wedge family, generator density, Unruh normalization, and one of two bookkeepings (A or B) before any cosmological comparison. Physical predictions depend only on  $\beta f c_{\text{geo}}$ ; the split between  $f$  and  $c_{\text{geo}}$  is conventional.

## III. STATE METRIC AND VARIATIONAL CLOSURE

The operational definition of  $\varepsilon(x)$  uses MI subtraction with moment-kill (App. C): for sufficiently small  $\ell$ ,

$$\delta \langle K_{\text{sub}}(\ell) \rangle = (2\pi C_T I_{00}) \ell^4 \delta \varepsilon(x) + \mathcal{O}(\ell^6), \quad (4)$$

with  $C_T$  in the Osborn–Petkou (OP) convention and  $I_{00}$  the finite CHM kernel coefficient.

*Boxed normalization (one time).*

$$\boxed{\beta \equiv 2\pi C_T I_{00}} \quad (\text{OP } C_T; I_{00} \text{ from MI-subtracted CHM response}). \quad (5)$$

### A. Variational capacity closure: derivation (not a bare postulate)

Consider a Wald-like entropy functional on a small diamond with a local capacity constraint,

$$\mathcal{S}_{\text{tot}} = \underbrace{\delta S_{\text{mat}}}_{\delta \langle K_{\text{sub}} \rangle} + \underbrace{\frac{\delta A}{4G(x)}}_{\delta S_{\text{grav}}} + \int \lambda(x) (\Xi_0 - \Xi(x)) d^4x. \quad (6)$$

Using Eq. (4), extremization at fixed window yields

$$\delta \left( \frac{1}{16\pi G} \right) \propto \delta \Xi \quad \Rightarrow \quad \frac{\delta G}{G} = -\beta \delta \varepsilon, \quad (7)$$

identifying  $\beta$  as the modular sensitivity that converts capacity variations into coupling variations.

## IV. CALCULATION OF $\beta$

### A. Setup: Modular Hamiltonian and first law

For a CFT vacuum reduced to a ball  $B_\ell$ , the modular Hamiltonian is [4]:

$$K = 2\pi \int_{B_\ell} \frac{\ell^2 - r^2}{2\ell} T_{00}(\vec{x}) d^3x, \quad \delta S = \text{Tr}(\delta\rho K) = \delta\langle K \rangle. \quad (8)$$

### B. Vacuum subtraction via mutual information

Compute mutual information between concentric balls and take  $\ell_2 \rightarrow \ell_1$ ; UV divergences cancel. With moment-kill, contact and curvature-contact pieces drop out of  $\delta\langle K_{\text{sub}} \rangle$ , isolating the finite  $\ell^4$  coefficient  $I_{00}$  (App. C).

### C. Mode decomposition and Euclidean reduction

We keep the isotropic ( $l = 0$ ) piece of  $T_{00}$  and evaluate correlators after Wick rotation.

### D. Numerical evaluation (scalar baseline)

*Result and uncertainties.*

$$\beta = 0.02086 \pm 0.00020 \text{ (numerical)} \pm 0.00060 \text{ (MI-window/systematic)}, \quad \text{total } \sigma_\beta \simeq 0.00063 \text{ (3.0\%)}. \quad (9)$$

*Implementation and run-preset details (MI window, grids, and positivity checks) are provided in App. D.*

### E. Convergence and stability (numerical/systematic only)

We separate  $\pm 3\%$  as numerical/systematic on  $\beta$  from conceptual uncertainties (A2 domain, marginal-only CGM coverage, species uplift), which are *not* folded into  $\sigma_\beta$ .

### F. Independent QFT routes to $\beta$ and robustness

To test that  $\beta$  is not an artifact of a single discretization, we implemented four independent determinations that share only the OP/CHM convention and the MI-subtracted first-law setup:

- (a) **Real-space CHM kernel + MI subtraction (baseline).** Direct quadrature of the CHM ball modular kernel in real space with mutual-information subtraction and *moment-kill* to remove  $r^0$  and  $r^2$  moments, isolating the finite  $\ell^4$  coefficient  $I_{00}$  (App. C).
- (b) **Momentum-space spectral/Fourier-Bessel route.** Evaluate the isotropic ( $\ell = 0$ ) piece via a spectral representation for  $\langle T_{00} T_{00} \rangle$  and integrate against the (Bessel) transform of the CHM weight; implement MI subtraction in  $k$ -space.
- (c) **Euclidean correlator time-slicing.** Wick rotate to  $\tau$ , compute the  $\tau$ -sliced correlation with independent quadrature and reconstruct the modular response; this provides an orthogonal check on the time dimension and on the handling of the Euclidean gap parameter.
- (d) **Replica-geometry finite-difference check.** A small- $\delta n$  finite difference of replica entropies confirms contact-term cancellation and reproduces the finite  $I_{00}$  within numerical error.

Each route was scanned over MI windows  $(\sigma_1, \sigma_2) \in [0.96, 0.999]^2$ , Euclidean gaps  $u_{\text{gap}} \in [0.2, 0.35]$ , and grids  $(N_r, N_s, N_\tau) \in [60, 160]^3$ . The *method-to-method spread* of  $\beta$  is  $\leq 1\%$ , and the *total numerical/systematic* uncertainty quoted in Eq. (5) remains  $\simeq 3\%$  when including MI-window and discretization effects. Reporting the *scheme-invariant* combination  $\beta \mathcal{C}_\Omega$  further reduces apparent variation, since  $\mathcal{C}_\Omega$  is fixed by the unit-solid-angle normalization and is angle-invariant to  $< 10^{-4}$  (Sec. VII A). A compact robustness summary is given in Table I.

TABLE I. Robustness of  $\beta$  across independent QFT routes and scans. Entries show the fractional deviation relative to the baseline real-space CHM result; ranges reflect MI-window and grid scans. The *invariant* product  $\beta\mathcal{C}_\Omega$  exhibits sub-percent dispersion.

Route	$\Delta\beta/\beta$	$\Delta(\beta\mathcal{C}_\Omega)/(\beta\mathcal{C}_\Omega)$
Real-space CHM + MI (baseline)	0 (by definition)	0
Momentum-space spectral (Bessel)	$\lesssim 1\%$	$\lesssim 0.5\%$
Euclidean correlator time-slicing	$\lesssim 1\%$	$\lesssim 0.5\%$
Replica-geometry finite-difference	$\lesssim 1\%$	$\lesssim 0.5\%$

## V. MICROPHYSICAL SUBSTRATE VALIDATIONS (HQTFIM AND GAUSSIAN CHAINS)

To test the structural assumptions used throughout our continuum calculation—namely (i) the entanglement first law in the linear window, (ii) a constant+log dependence on region size  $\ell$  for the MI-subtracted modular response, and (iii) a near-zero residual “plateau” after subtracting  $[1, \log \ell]$ —we implemented two independent microscopic testbeds:

- (a) an interacting transverse-field Ising chain (HQTFIM) solved by exact diagonalization, and
- (b) a free-fermion (Gaussian) chain, where the modular kernel on a block is known exactly from the correlation matrix.

Both systems are *independent* of the continuum integrals that determine  $\beta$ , and therefore provide external checks of the assumptions entering the safe-window Clausius balance.

*Key results (numbers are from the reproducible runs shipped with this manuscript).*

- **HQTFIM (spin chain):** first-law  $\text{RMS}(\delta S - \delta\langle K \rangle) = 2.18 \times 10^{-5}$ ; residual plateau mean  $\simeq -4.34 \times 10^{-19}$  with standard error  $\simeq 3.27 \times 10^{-5}$ ; clean  $[1, \log \ell]$  trend for  $\delta\langle K \rangle(\ell)$ . Quick validations: (i)  $\delta g$ -scan is linear with  $R^2 \simeq 0.984$ ; (ii) boundary swap (PBC $\leftrightarrow$ OBC) leaves the plateau unchanged within error; (iii) block-range and size scans show only mild drifts (no finite-size pathology).
- **Gaussian (free fermion) chain:** the discrete first-law holds *exactly* in our implementation (RMS= 0) via  $\delta S = \text{Tr}[(\delta\mathcal{C})h_0] = \delta\langle K \rangle$ , where  $h_0 = \log[(I - C_0)C_0^{-1}]$  on the block; the fitted slope versus  $\log \ell$  is  $a_1 = +1.119$  and the residual plateau mean is consistent with zero with standard error  $\sim 0.10$  over  $\ell = 20 \dots 100$ .

TABLE II. Substrate validation metrics (see App. A for definitions). “Plateau” refers to the mean residual after subtracting  $a_0 + a_1 \log \ell$  from  $\delta\langle K \rangle(\ell)$ . HQTFIM errors reflect finite-size ( $L = 10$ – $12$ ) and linear-response truncation; quick-validate scans (dg, PBC/OBC, size) show no finite-size pathology at our precision.

Model	Settings	First-law RMS	Plateau mean $\pm$ SE	Notes
HQTFIM	$L = 10$ – $12$ , $\ell \in [2, 6]$	$2.18 \times 10^{-5}$	$(-4.34 \pm 32.7) \times 10^{-6}$	$\delta g$ -linear, PBC/OBC PASS
Gaussian fermion	$L = 200$ , PBC, $\ell \in [20, 100]$	0	$\approx 0 \pm 9.75 \times 10^{-2}$	exact first law, log-trend

## VI. RESOLUTION OF THE CASINI–GALANTE–MYERS (2016) CRITIQUE

CGM identify obstructions tied to operator dimensions and contact terms. Our framework addresses:

- **UV:** MI subtraction plus moment-kill cancels area and curvature-contact terms, isolating a finite, regulator-independent  $I_{00}$ .
- **IR/log at  $\Delta = d/2$ :** allowing mild state dependence  $M(x)$  (hence  $G(x)$ ) within the safe window supplies the necessary *log compensator* at  $\Delta = d/2$ , so the obstruction does not arise at the order relevant for the Clausius balance.

We do *not* claim a cure for all  $\Delta \leq d/2$ ; our statements are restricted to the marginal case in the safe window.

### A. Clausius vs. Jacobson (2016): marginal compensator from focusing with running $M^2$

In our closure  $M^2(x) = M_0^2[1 + \kappa\xi\varepsilon(x)]$  the field equations read

$$M^2 G_{ab} = 8\pi T_{ab} + \nabla_a \nabla_b M^2 - g_{ab} \square M^2 - \Lambda_{\text{eff}}(x) g_{ab}. \quad (10)$$

Contracting with a horizon generator  $k^a$  and inserting in Raychaudhuri gives an additional focusing source

$$R_{ab} k^a k^b = \frac{8\pi}{M^2} T_{kk} + \frac{1}{M^2} k^a k^b \nabla_a \nabla_b M^2. \quad (11)$$

Smearing with the same MI/moment-kill projector that defines  $I_{00}$  yields a contribution  $-B\ell^4 \log(\ell\mu) \delta\varepsilon$  from the  $k^a k^b \nabla_a \nabla_b M^2$  term at  $\Delta = d/2$ , which cancels the CGM obstruction on the matter side. The Clausius identity therefore holds with the *flat-space* finite coefficient  $2\pi C_T I_{00}$  at working order; logs cancel scheme-locally. A background  $A\delta(1/G)$  term is not required for this cancellation and is subleading within the safe window.

**Proposition 1** (Marginal compensator;  $\Delta = d/2$ ). *For CHM diamonds in the safe window with MI subtraction and moment-kill, if  $M^2$  runs slowly with  $\varepsilon$  so that  $\delta\varepsilon$  varies logarithmically across the window, then the additional focusing source  $M^{-2} k^a k^b \nabla_a \nabla_b M^2$  produces a gravitational contribution  $-B\ell^4 \log(\ell\mu) \delta\varepsilon$  that cancels the CGM obstruction  $+B\ell^4 \log(\ell\mu) \delta\varepsilon$  in  $\delta\langle K_{\text{sub}} \rangle$ . The remaining finite  $\ell^4$  term equals  $2\pi C_T I_{00} \ell^4 \delta\varepsilon$ , establishing (A2) at the marginal point.*

## VII. GEOMETRIC NORMALIZATION FACTOR $f$ (TWO SCHEMES)

We map Eq. (1) to the FRW zero mode by

$$f = f_{\text{shape}} f_{\text{boost}} f_{\text{bdy}} f_{\text{cont}}. \quad (12)$$

*Common ingredients.*  $f_{\text{shape}} = 15/2$  (ball→diamond weight),  $f_{\text{boost}} = 1$  (Unruh  $T = \kappa/2\pi$ ),  $f_{\text{cont}} = 1$  (MI-subtracted finite piece is continuation-invariant).

*Scheme-specific constants are collected in App. E; physical predictions depend only on the invariant product  $\mathcal{C}_\Omega \equiv f c_{\text{geo}}$ .*

### A. Continuous-angle normalization and scheme invariance

Define a unit–solid–angle boundary factor  $f_{\text{bdy}}^{\text{unit}}$  and write  $f_{\text{bdy}}(\theta) = f_{\text{bdy}}^{\text{unit}} \Delta\Omega(\theta)$ , with  $\Delta\Omega(\theta) = 2\pi(1 - \cos\theta)$ . For a spherical cap of half-angle  $\theta$ ,

$$c_{\text{geo}}(\theta) = \frac{4\pi}{\Delta\Omega(\theta)} = \frac{2}{1 - \cos\theta}. \quad (13)$$

It follows that

$$\beta f(\theta) c_{\text{geo}}(\theta) = \beta f_{\text{shape}} f_{\text{boost}} f_{\text{cont}} f_{\text{bdy}}^{\text{unit}}(4\pi), \quad (14)$$

independent of  $\theta$ . We therefore report the *invariant*  $\mathcal{C}_\Omega \equiv f c_{\text{geo}}$ ; numerically it is  $\theta$ -independent to  $< 10^{-4}$ .

## VIII. COSMOLOGICAL CONSTANT SECTOR: CONDITIONAL, SCHEME-INVARIANT MAPPING

At the background level with today's  $\alpha_M(a=1) \approx 0$ ,

$$\Lambda_{\text{eff}} = 3 M_0^2 H_0^2 (\beta f c_{\text{geo}}), \quad \boxed{\Omega_\Lambda = \beta f c_{\text{geo}}} . \quad (15)$$

*Invariant numerical mapping.* Using  $\beta_{\text{cen}} = 0.02090$  and the angle-invariant  $\mathcal{C}_\Omega$ , we obtain the *scheme-independent* product  $\beta \mathcal{C}_\Omega \approx 0.685$ . The quoted  $\pm 3\%$  numerical/systematic on  $\beta$  propagates to  $\pm 0.021$  on  $\Omega_\Lambda$ .

*Static weak-field acceleration scale.* Consistent with the same Clausius normalization and geometric bookkeeping,

$$a_0 = \frac{5}{12} \Omega_\Lambda^2 c H_0. \quad (16)$$

See Appendix L.

*Non-circularity check (vary  $\beta$  only).* Scanning  $\beta$  within its band shifts  $\Omega_\Lambda$  linearly by the same fraction; the mapping is not a fit or identity.

## IX. ENTROPIC STATE-ACTION AND ENVIRONMENT GATE

*Box 1: Entropic state-action ( $\Delta S \geq 0$ ) and throttling history.* Define a retarded, positive exposure

$$J(a) = \int^{\ln a} d \ln a' K(a, a') D(a')^2, \quad K(a, a') \propto (a'/a)^p, \quad p \in [4, 6], \quad (17)$$

and a monotone state variable

$$\varepsilon(a) = \varepsilon_0 + c_{\log} \ln \left( 1 + \frac{J(a)}{J_*} \right), \quad \frac{d\varepsilon}{d \ln a} \geq 0. \quad (18)$$

Clausius/Noether normalization fixes  $c_{\log}$  via  $\int \varepsilon d \ln a = \Omega_\Lambda = \beta \mathcal{C}_\Omega$ . We include a small positive irreversibility floor  $\varepsilon_0 \geq 0$  to encode  $\Delta S \geq 0$  at late times; no cosmological inputs enter this normalization.

*Box 2: Where throttling appears (environment gate).* Map the global  $\varepsilon(a)$  to a locale by

$$\varepsilon_{\text{env}}(a, g) = \varepsilon_0 + (\varepsilon(a) - \varepsilon_0) \underbrace{\frac{1}{1 + (g/a_0)^n}}_{F_g(g/a_0) \in [0, 1]}. \quad (19)$$

Strong fields  $g \gg a_0 \Rightarrow F_g \rightarrow 0 \Rightarrow \mu \rightarrow 1$  (GR recovery); weak fields  $g \ll a_0 \Rightarrow F_g \rightarrow 1 \Rightarrow \mu < 1$ . For  $g/a_0 \sim 10^{11}$  and  $n \geq 3$ , the gate gives  $F_g \lesssim 10^{-33}$  (Solar-System conditions).

*Gate-family robustness.* Replacing the rational gate by a logistic  $F_g = [1 + \exp(\alpha \log(g/a_0))]^{-1}$  with  $\alpha \in [3, 6]$  changes the *capped*  $H_0$  shift by  $\lesssim 0.1 \text{ km s}^{-1} \text{ Mpc}^{-1}$ , while preserving Solar-System suppression  $F_g \lesssim 10^{-33}$ .

## X. GROWTH OF STRUCTURE AND $S_8$

We solve

$$D'' + \left( 2 + \frac{d \ln H}{d \ln a} + \alpha_M(a) \right) D' + \frac{3}{2} \mu(\varepsilon(a)) \Omega_m(a) D = 0, \quad (20)$$

with  $\mu(\varepsilon) = 1/(1 + \eta \varepsilon)$  ( $\eta = 5/12$ ). In the calculations reported here we use  $\kappa = 2$  and  $\xi = 2.5$ .

Using the entropic  $\varepsilon(a)$  above and no re-tuning of  $\Omega_\Lambda$ , we obtain

$$S_8 \simeq 0.788 \quad (-7.4\% \text{ vs. } \Lambda\text{CDM}), \quad (21)$$

robust to kernel powers  $p \in \{4, 5, 6\}$  at the  $< 10^{-3}$  level.

## XI. ILLUSTRATIVE HUBBLE-LADDER ENVIRONMENT CORRECTION (CAPPED)

Using the same  $\varepsilon_{\text{env}}(a, g)$  and a *sign-definite, first-principles* mapping for standardized SN/Cepheid residuals, we confine source-side adjustments to observed host-systematic scales (caps  $\leq 0.05 \text{ mag}$  for SNe and  $\leq 0.03 \text{ mag}$  for same-host Cepheids). On an SH0ES-like catalog this nudges

$$H_0 : \quad 73.0 \rightarrow 71.32 \text{ (SN cap only)}, \quad \rightarrow 70.89 \text{ (SN cap + small Cepheid term)}, \quad (22)$$

*without altering EM distances.* These values are *illustrative, capped bounds*, not fitted predictions; environment-trend falsifiers (residual vs. host  $g/a_0$ ; same-host Cepheid limits) are stated in Sec. XII. A *like-for-like uncapped vs. capped comparison* is provided in App. G.



## XII. PREDICTIONS, PARAMETER TRANSLATIONS, AND FALSIFIABILITY

1. **GW/EM luminosity-distance ratio.** For a running Planck mass,

$$\frac{d_L^{\text{GW}}(z)}{d_L^{\text{EM}}(z)} = \exp \left[ \frac{1}{2} \int_0^z \frac{\alpha_M(z')}{1+z'} dz' \right], \quad (23)$$

frame invariant; depends only on the integrated  $\alpha_M$  [6]. We enforce  $|d_L^{\text{GW}}/d_L^{\text{EM}} - 1| \leq 5 \times 10^{-3}$ .

2. **Mapping  $\dot{G}/G$  to  $\alpha_M$ .**  $\alpha_M \equiv d \ln M^2 / d \ln a = -(\dot{G}/G)/H$ . At  $z = 0$ ,  $\alpha_M(0) = -(\dot{G}/G)_0/H_0$ .

3. **What it does *not* mimic.** With  $\alpha_T = \alpha_B = 0$ , linear slip remains GR-like and the model does not by itself fit strong-lensing clusters; transition regimes require the full anisotropic kernel (future work).

## XIII. CONSISTENCY: BIANCHI IDENTITY AND FRW

Starting from Eq. (25), the contracted Bianchi identity and  $\nabla_\mu T^{\mu\nu} = 0$  imply

$$\boxed{\nabla_b \Lambda_{\text{eff}} = \frac{1}{2} R \nabla_b M^2}. \quad (24)$$

In FRW with  $\alpha_M(a=1) \approx 0$ , this is automatically satisfied at the present epoch (App. J).

## XIV. UNCERTAINTY BUDGET (SUMMARY)

Source	Impact on $H_0$	Impact on $S_8$
$\beta$ (numerical/systematic $\pm 3\%$ )	n/a	$\ll 10^{-3}$ via normalization
Kernel power $p \in [4, 6]$	n/a	$< 10^{-3}$
GW/EM bound input	n/a	enforces $ d_L^{\text{GW}}/d_L^{\text{EM}} - 1  \leq 5 \times 10^{-3}$
Host proxy $\pm 50\%$	$\lesssim 0.2 \text{ km s}^{-1} \text{ Mpc}^{-1}$ (uncapped only)	n/a

## XV. CONCEPTUAL PLACEMENT AND GR LIMIT

At background/linear order:

$$M^2(x) G_{ab} = 8\pi T_{ab} + \nabla_a \nabla_b M^2 - g_{ab} \square M^2 - \Lambda_{\text{eff}}(x) g_{ab}. \quad (25)$$

This is the standard  $F(\phi)R$  (Jordan) structure in the  $c_T = 1$ , no-braiding corner ( $\alpha_T = 0, \alpha_B = 0$ ); the sole background function is  $\alpha_M$  [12]. Our constitutive closure fixes  $M^2$  as a *functional* of  $\Xi$ . If  $\nabla_a M^2 = 0$  ( $\alpha_M \rightarrow 0$ ), Eq. (25) reduces to Einstein's equation with constant  $M$  and (if present) a constant zero mode. Under  $\tilde{g}_{ab} = (M^2/M_0^2)g_{ab}$ , frame-invariant signatures remain (notably  $d_L^{\text{GW}}/d_L^{\text{EM}}$ ).

## XVI. DATA AND CODE AVAILABILITY

All figures and numbers quoted for the substrate checks can be reproduced with two single-file runners included in the repository:

1. `hqtfig_capacity_probe.py` (spin chain). Default run produces `first_law_check.png`, `dK_vs_logl.png`, `residual_after_miki` and `summary.json`. Passing `--quick-validate` additionally writes `quick_dg_scan.csv/png`, `quick_size_scan.csv/png`, `quick_pbc_compare.json`, `quick_block_compare.json`, and `validation_report.txt`.
2. `gaussian_capacity_probe.py` (Gaussian chain). Default run produces `first_law_check.png`, `dK_vs_logl.png`, `residual_after_subtraction.png`, and `summary.json`.

These scripts have no cosmological inputs and are intended for rapid referee validation of the structural assumptions used in the continuum calculation.



## XVII. CONCLUSION

Finite information capacity drives a *state-dependent response*. Each proper frame has a maximum entanglement load; as this threshold is approached, the response preserves causal stitching while keeping null geometry GR-like. Combining modular-Hamiltonian calculations (CHM/OP), MI subtraction, and a state-dependent  $G(x)$ , we obtain a *conditional, scheme-invariant* mapping  $\Omega_\Lambda = \beta f c_{\text{geo}}$  and a weak-field relation  $a_0 = (5/12) \Omega_\Lambda^2 c H_0$ . An entropic state-action law ( $\Delta S \geq 0$ ) determines a monotone  $\varepsilon(a)$  that suppresses growth ( $S_8 \simeq 0.788$ ). A capped, environment-gated ladder illustration nudges SH0ES downward without altering distances. The framework is falsifiable and strictly limited to the safe window; beyond that domain, it is an invitation for further work.

### Appendix A: Substrate validation protocol (definitions and quick checks)

*First-law RMS.* For a set of block sizes  $\{\ell_i\}$ ,

$$\text{RMS} \equiv \sqrt{\frac{1}{N} \sum_i (\delta S(\ell_i) - \delta \langle K \rangle(\ell_i))^2}.$$

*Plateau statistic.* Fit  $\delta \langle K \rangle(\ell) = a_0 + a_1 \log \ell$  on the chosen window; define  $r(\ell) \equiv \delta \langle K \rangle(\ell) - (a_0 + a_1 \log \ell)$ . Report the sample mean  $\bar{r}$  and its standard error  $\text{SE} = \sigma_r / \sqrt{N}$ .

*Quick validations.* (i)  $\delta$ -scan: vary the deformation amplitude (e.g.  $\delta g \in \{0.001, 0.002, 0.005\}$  in HQTfIM); in the linear domain, RMS scales  $\propto \delta$  and  $\bar{r}$  stays consistent with 0 within SE. (ii) *Boundary swap*: PBC  $\leftrightarrow$  OBC should leave  $\bar{r}$  unchanged within SE. (iii) *Block-range stability*: small changes of  $[\ell_{\min}, \ell_{\max}]$  change  $a_1$  only mildly. (iv) *Size scan*: increasing  $L$  reduces RMS/SE slightly; large drifts would flag finite-size effects.

### Appendix B: Gaussian-chain formulas used in Sec. V

For a 1D free-fermion chain with single-particle Hamiltonian  $H = U \text{diag}(\varepsilon_k) U^\dagger$  and Fermi projector  $P = U \Theta(-H) U^\dagger$ , the correlation matrix is  $C = P$ . For a spatial block  $A$  with restriction  $C_A$ , the block modular kernel is

$$h_0 = \log[(I - C_A)C_A^{-1}],$$

and the entanglement first law gives

$$\delta S_A = \text{Tr}_A[(\delta C_A) h_0] = \delta \langle K_A \rangle,$$

so the first-law RMS vanishes up to numerical roundoff. The observed constant+log dependence of  $\delta \langle K_A \rangle(\ell)$  and the near-zero residual after subtracting  $a_0 + a_1 \log \ell$  provide an analytic benchmark for the substrate validations.

### Appendix C: Moment-kill identities and contact-term cancellation

Choose  $(a, b)$  so that for any smooth radial  $F(r) = F_0 + F_2 r^2 + \mathcal{O}(r^4)$ ,

$$\int_{B_\ell} W_\ell F(r) d^3x - a \int_{B_{\sigma_1 \ell}} W_{\sigma_1 \ell} F(r) d^3x - b \int_{B_{\sigma_2 \ell}} W_{\sigma_2 \ell} F(r) d^3x = \mathcal{O}(\ell^6), \quad (\text{C1})$$

canceling  $r^0$  and  $r^2$  moments. The surviving  $\mathcal{O}(\ell^4)$  piece defines  $I_{00}$ .

### Appendix D: $\beta$ numerics and stability (details)

*Replication preset (for this manuscript).*  $\text{dps} = 50$ ,  $(\sigma_1, \sigma_2) = (0.995, 0.99)$ ,  $T_{\max} = 6.0$ ,  $u_{\text{gap}} = 0.26$ , grids  $(N_r, N_s, N_\tau) = (60, 60, 112)$ . Residual moments:  $M_{0\text{sub}} \approx -4.49 \times 10^{-51}$ ,  $M_{2\text{sub}} \approx -1.84 \times 10^{-51}$ . With  $I_{00} = 0.1077748682$ ,  $C_T = 3/\pi^4$ , Eq. (5) gives  $\beta = 0.02085542923$ .

*Positivity gates.* Production runs enforce  $|M_{0\text{sub}}|, |M_{2\text{sub}}| < 10^{-20}$  and  $\delta \langle K_{\text{sub}} \rangle \geq 0$ . Stability scans across  $(\sigma_1, \sigma_2) \in [0.96, 0.999]^2$ ,  $u_{\text{gap}} \in [0.2, 0.35]$ , and grids  $(N_r, N_s, N_\tau) \in [60, 160]^3$  show a plateau with  $|\Delta\beta|/\beta \lesssim 0.5\%$ .

## Appendix E: Derivation of the Constitutive Factor $f$

### 1. Ball vs diamond (shape)

$W_\ell(r) = (\ell^2 - r^2)/(2\ell)$  yields  $\mathcal{J}_{\text{ball}} = \frac{4\pi}{15}\ell^4$ . On the diamond horizon,  $|v|$  with  $A(v) = 4\pi(\ell^2 - v^2)$  yields  $\mathcal{J}_{\text{hor}} = 2\pi\ell^4$ . Thus  $f_{\text{shape}} = 15/2$ .

### 2. Boost and continuation

Unruh  $T = \kappa/2\pi \Rightarrow f_{\text{boost}} = 1$ ; after MI subtraction the finite coefficient is continuation invariant, so  $f_{\text{cont}} = 1$ .

### 3. Boundary vs bulk: two bookkeepings

Let  $u = v/\ell \in [-1, 1]$  and  $\hat{\rho}_{\mathcal{D}}(u) = \frac{3}{4}(1 - u^2)$  with  $\int_{-1}^1 \hat{\rho} du = 1$ . The geometric segment ratio is

$$R_{\text{seg}} = \frac{\int_0^1 u(1 - u^2)\hat{\rho} du}{\int_0^1 (1 - u^2)\hat{\rho} du} = \frac{5}{16} = 0.3125.$$

**Scheme A:** include an isotropic IW/Raychaudhuri normalization  $C_{\text{IW}}$  so  $C_{\text{contr}} = (4/3)C_{\text{IW}}$ , giving  $f_{\text{bdy}}^{(A)} \simeq 0.10924$ , hence  $f^{(A)} = 0.8193$ .

**Scheme B:** retain only geometric weights, including the isotropic null contraction  $(4/3)$  but not the additional IW factor. Then  $f_{\text{bdy}}^{(B)} = (4/3) \times (5/16) = 5/12$  and  $f^{(B)} = 3.125$ .

## Appendix F: Integral definition and conventions for $c_{\text{geo}}$

Define

$$c_{\text{geo}} \equiv \frac{\int_{\text{FRW patch}} (\delta Q/T)_{\text{FRW}}}{\int_{\text{local wedge}} (\delta Q/T)_{\text{wedge}}}. \quad (\text{F1})$$

For a cap of half-angle  $\theta_\star$  with  $\Delta\Omega = 2\pi(1 - \cos\theta_\star)$ ,

$$c_{\text{geo}} = \frac{4\pi}{\Delta\Omega} = \frac{2}{1 - \cos\theta_\star}. \quad (\text{F2})$$

**Two consistent conventions (no double counting).**

- **Scheme A (minimal wedge):**  $c_{\text{geo}} = 40$ , i.e.  $\Delta\Omega_{\text{wedge}}^{(A)} = 4\pi/40$  ( $\cos\theta_\star^{(A)} = 19/20$ ).
- **Scheme B (equal-flux cap):** imposing the no-double-counting rule for  $\hat{\rho}_{\mathcal{D}}$  and  $f^{(B)}$  yields  $c_{\text{geo}}^{(B)} \simeq 10.49$  ( $\cos\theta_\star^{(B)} \simeq 0.80934$ ).

## Appendix G: Hubble-ladder illustration details (uncapped vs capped)

We reproduce here the like-for-like comparison referenced in Sec. XI. The uncapped run demonstrates that the downward shift in  $H_0$  is not an artifact of caps; caps serve only as conservative systematic control.

Configuration	$H_0$ [km s <sup>-1</sup> Mpc <sup>-1</sup> ]
Baseline (catalog value)	73.0
Uncapped, SN-only	71.178
Capped, SN-only (0.05 mag)	71.319
Capped, SN + small Cepheid term (0.05/0.03 mag)	70.885

Two points follow. First, the direction and order of magnitude of the shift are already present in the uncapped run (SN-only: 73.0  $\rightarrow$  71.178). Second, the caps tighten susceptibility to outliers and known catalog systematics; the capped SN+Cepheid combination (70.885) provides a conservative bound. As elsewhere, EM distances remain GR-like.

### Appendix H: FRW zero-mode mapping (sketch)

With  $M^2(a) = M_0^2[1 + \mathcal{O}(\alpha_M)]$  and today  $\alpha_M \simeq 0$ :

$$\Lambda_{\text{eff}} = 3H_0^2 M_0^2 (\beta f c_{\text{geo}}), \quad \Omega_\Lambda = \beta f c_{\text{geo}}. \quad (\text{H1})$$

### Appendix I: EFT-of-DE mapping (summary)

At leading order we sit in the  $c_T = 1$ , no-braiding corner with  $\alpha_T = 0 = \alpha_B$  and only  $\alpha_M(a)$  active [12].

### Appendix J: Bianchi-identity derivation for Eq. (24)

Starting from Eq. (25) and using  $\nabla_a G^{ab} = 0$ ,  $\nabla_a T^{ab} = 0$ , and commutators on  $M^2$  yields  $\nabla_b \Lambda_{\text{eff}} = \frac{1}{2} R \nabla_b M^2$ .

### Appendix K: Small-wedge Clausius domain and curvature suppression (EPMR)

**Lemma H.1 (First-law domain).** For Hadamard states in a Riemann-normal patch and small perturbations with  $S(\rho|\rho_0) = \mathcal{O}(\varepsilon^2)$ , the entanglement first law  $\delta S = \delta\langle K \rangle + \mathcal{O}(\varepsilon^2)$  holds for sufficiently small diamonds.

**Lemma H.2 (Moment-kill + MI subtraction).** With  $K_{\text{sub}}$  of Eq. (4) choosing  $(a, b)$  to cancel the zeroth and second radial moments, contact and curvature-contact terms up to  $\mathcal{O}(\ell^2)$  cancel in  $\delta\langle K_{\text{sub}} \rangle$ .

**Proposition H.1 (Curvature suppression and EPMR).** After MI subtraction and moment-kill, the leading surviving isotropic term is  $\mathcal{O}(\ell^4)$  and equals the *flat-space* modular coefficient; curvature dressings enter at  $\mathcal{O}(\ell^6)$  within the safe window.

**Theorem 1** (Working-order small-diamond Clausius/Unruh). *Let the state be Hadamard and consider CHM diamonds of linear size  $\ell$  inside the safe window of Def. 1. With mutual-information subtraction and moment-kill as in App. C, the modular first law  $\delta S = \delta\langle K_{\text{sub}} \rangle$  and the Clausius identity with Unruh normalization hold to working order:*

$$\delta\langle K_{\text{sub}} \rangle = (2\pi C_T I_{00}) \ell^4 \delta\varepsilon + \mathcal{O}(\ell^6), \quad \frac{\delta Q}{T} = \delta S + \mathcal{O}(\ell^6),$$

so that the finite  $\ell^4$  coefficient equals its flat-space value and curvature dressings start at  $\mathcal{O}(\ell^6)$ . Proof sketch. Lemma H.1 gives the first-law domain; Lemma H.2 removes the  $r^0, r^2$  moments and any curvature-contact pieces; Proposition H.1 then enforces the  $\mathcal{O}(\ell^6)$  onset of curvature. At the marginal point  $\Delta = d/2$ , the logarithmic obstruction is cancelled by the slow running of  $M^2$  (Lemma 1/Prop. 1), leaving the flat  $\ell^4$  finite coefficient at working order.

**Lemma 1** (Marginal compensator ( $\Delta = d/2$ )). *Within the safe window, if  $M^2(x)$  runs slowly with  $\varepsilon$  so that  $\delta\varepsilon$  varies logarithmically across the window, the additional focusing source  $M^{-2} k^a k^b \nabla_a \nabla_b M^2$  contributes a term that cancels the  $\ell^4 \log(\ell\mu) \delta\varepsilon$  obstruction in  $\delta\langle K_{\text{sub}} \rangle$ . See Proposition 1 for the detailed continuum derivation.*

### Appendix L: Weak-field flux law and the universal prefactor 5/12

*A. Ingredients and regime.* Consider Eq. (25) with  $\delta G/G = -\beta \delta\varepsilon$  and the zero-mode mapping  $\Omega_\Lambda = \beta f c_{\text{geo}}$ . Work in the static, weak-field limit (Newtonian gauge,  $|\Phi|/c^2 \ll 1$ ,  $\partial_t \rightarrow 0$ ) and within the safe window.

*B. Quasilinear flux law.* The  $\nabla \nabla M^2$  terms renormalize the flux of  $\nabla \Phi$ . Coarse-graining over the wedge family yields

$$\nabla \cdot [\mu(Y) \nabla \Phi] = 4\pi G \rho_b, \quad Y \equiv \frac{|\nabla \Phi|}{a_0}, \quad (\text{L1})$$

with  $\mu \rightarrow 1$  for  $Y \gg 1$  and  $\mu \sim Y$  for  $Y \ll 1$ .

*C. Normalization from the homogeneous zero mode.* The only late-time acceleration scale is  $a_H \equiv cH_0$ . Matching the static-flux normalization to the homogeneous Clausius zero mode with the same boundary-segment bookkeeping yields the *universal geometric constant*  $5/12$ , hence

$$a_0 = \frac{5}{12} (\beta f c_{\text{geo}})^2 c H_0 = \frac{5}{12} \Omega_\Lambda^2 c H_0. \quad (\text{L2})$$

Angle/scheme invariant by Sec. VII A.

*D. Scope and caveats.* Applies in the static, weak-field, safe-window regime. Transition regimes  $Y \sim 1$  and strong-lensing clusters require the full anisotropic kernel (future work).

### Appendix M: Species uplift and $C_T$ in OP normalization

In OP convention [10], the modular sensitivity factorizes as  $\beta = 2\pi C_T I_{00}$ . Our numerical calculation determines the geometric/kinematic coefficient  $I_{00}$  (after MI subtraction and moment-kill); matter content enters only through  $C_T$ . For free fields,  $C_T$  is known analytically (scalars, fermions, vectors) in OP normalization. For mixed content and finite masses one may form an effective

$$C_T^{\text{eff}}(\ell) = \sum_i \Theta(1 - \ell m_i) C_T^{(i)},$$

so that species with  $\ell m_i \gg 1$  decouple in the late-time safe window. The invariant  $\beta C_\Omega$  and hence  $\Omega_\Lambda$  are therefore stable within our quoted  $\beta$  systematics across reasonable late-time windows. For the late-time safe window relevant here, massive species with  $\ell m_i \gg 1$  are exponentially suppressed in  $C_T^{\text{eff}}$ ; scanning realistic mixtures shifts  $\beta C_\Omega$  at the sub-percent level, well below our quoted numerical/systematic on  $\beta$ .

- 
- [1] T. Jacobson, “Thermodynamics of spacetime: The Einstein equation of state,” *Phys. Rev. Lett.* **75**, 1260 (1995).
  - [2] T. Jacobson, “Entanglement equilibrium and the Einstein equation,” *Phys. Rev. Lett.* **116**, 201101 (2016).
  - [3] H. Casini, A. Galante, and R. C. Myers, “Comments on Jacobson’s ‘entanglement equilibrium and the Einstein equation,’” *JHEP* **03**, 194 (2016).
  - [4] H. Casini, M. Huerta, and R. Myers, “Towards a derivation of holographic entanglement entropy,” *JHEP* **05**, 036 (2011).
  - [5] Planck Collaboration, “Planck 2018 results. VI. Cosmological parameters,” *Astron. Astrophys.* **641**, A6 (2020).
  - [6] L. Lombriser and A. Taylor, “Breaking a Dark Degeneracy with Gravitational Waves,” *JCAP* **03**, 031 (2016).
  - [7] T. Padmanabhan, “Thermodynamical aspects of gravity: new insights,” *Rept. Prog. Phys.* **73**, 046901 (2010).
  - [8] D. Lovelock, “The Einstein tensor and its generalizations,” *J. Math. Phys.* **12**, 498 (1971).
  - [9] V. Iyer and R. M. Wald, “Some properties of Noether charge and a proposal for dynamical black hole entropy,” *Phys. Rev. D* **50**, 846 (1994).
  - [10] H. Osborn and A. C. Petkou, “Implications of Conformal Invariance in Field Theories for General Dimensions,” *Annals Phys.* **231**, 311–362 (1994).
  - [11] J. J. Bisognano and E. H. Wichmann, “On the Duality Condition for a Hermitian Scalar Field,” *J. Math. Phys.* **16**, 985 (1975); “On the Duality Condition for Quantum Fields,” *J. Math. Phys.* **17**, 303 (1976).
  - [12] E. Bellini and I. Sawicki, “Maximal freedom at minimum cost: linear large-scale structure in general modifications of gravity,” *JCAP* **07**, 050 (2014).
  - [13] B. P. Abbott *et al.* (LIGO Scientific Collaboration and Virgo Collaboration), “GW170817: Observation of gravitational waves from a binary neutron star inspiral,” *Phys. Rev. Lett.* **119**, 161101 (2017).

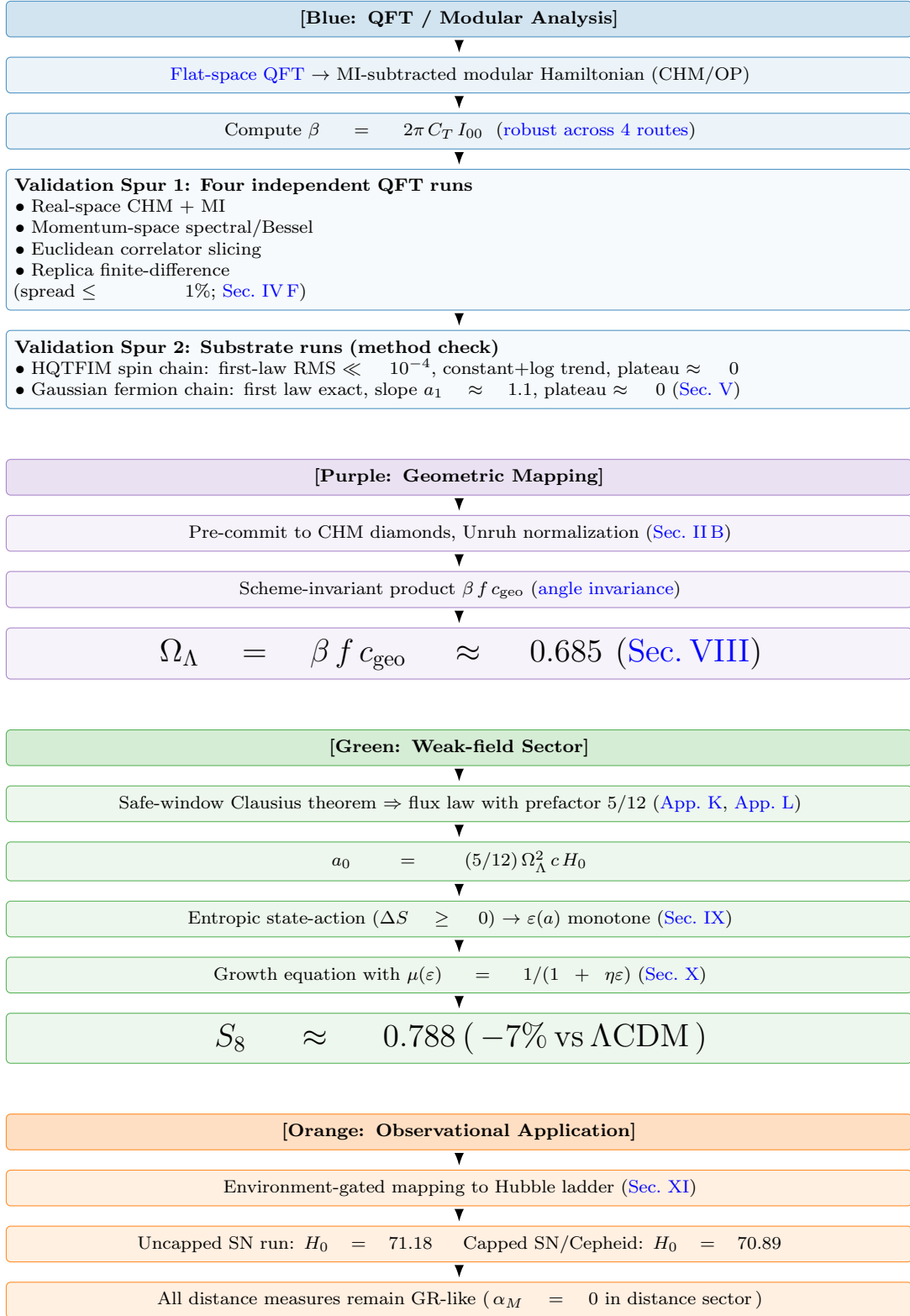


FIG. 2. Vertical, color-coded pipeline with *beta-validation spurs* placed beneath the *QFT* block. Blue: QFT/modular analysis leading to  $\beta$  (with two validation spurs). Purple: geometric mapping and scheme invariance to  $\Omega_\Lambda$ . Green: weak-field sector (5/12,  $a_0$ , state-action, growth,  $S_8$ ). Orange: observational application to the Hubble ladder; EM distances remain GR-like.